Antarct. Meteorite Res., **13**, 285–301, 2000

Mineralogy of Antarctic micrometeorites recovered from the Dome Fuji Station

Takaaki Noguchi[1] and Tomoki Nakamura[2]

[1] *Department of Materials and Biological Sciences, Ibaraki University, Bunkyo 2-chome, Mito 310–8512*

[2] *Earth and Planetary Sciences, Graduate School of Science, Kyushu University 33, Hakozaki, Fukuoka 812–8581*

Abstract: Mineralogy of six micrometeorites (MMs) was investigated by a TEM for electron petrography. These MMs were selected based on X-ray diffraction analysis by a Gandolfi X-ray camera, qualitative analysis by SEM-EDS of the surfaces of the MMs, and based on textural observation and quantitative analysis of "polished" sections of the MMs by a SEM and an EPMA. We found one saponite-bearing MM F96CI024 among 83 MMs. It has textural and mineralogical characteristics similar to a saponite-bearing MM BI 91/3-108. From the mineralogical point of view, they are different from CI, CM, CR, and hydrated CV chondrites. F96CI020 and F96DI021 contain lepidocrocite, which was formed by terrestrial weathering. MMs are susceptible to terrestrial weathering even in snow (or ice). A magnesium- and iron-bearing mineral (probably (Mg, Fe)O) was found in the phyllosilicate-bearing MM and two pyroxene-rich MMs. In the latter MMs, the mineral coexists with pyroxene that was formed newly during atmospheric entry of the MMs.

1. Introduction

Many micrometeorites (MMs) have experienced heating during atmospheric entry. Some of them were partially to totally melted ("scoriaceous" MMs). Others were not melted although affected thermally (unmelted MMs). There are unmelted MMs that contain phyllosilicates (*e.g.*, Kurat *et al.*, 1994; Klöck and Stadermann, 1994; Genge *et al.*, 1997). Six to sixteen percent of the unmelted MMs are thought to be phyllosilicate-bearing, based on their chemical compositions (Kurat *et al.*, 1992; Genge *et al.*, 1997). Chemical compositions of phyllosilicate-bearing unmelted MMs have the lithophile trace element abundance similar to CI, CM and CR chondrites (*e.g.*, Jessberger *et al.*, 1999). Based on mineralogy, there are two types among such MMs. First type is characterized by the existence of serpentine. MMs belonging to this type sometimes contain tochilinite-like mineral. The other type of MMs is characterized by the existence of saponite. A TEM study of an Antarctic MM (AMM) belonging to this type revealed that it contains only smectite (saponite) (Klöck and Stadermann, 1994).

The Japanese Antarctic Research Expedition (JARE) team recovered deposits in a water tank at the Dome Fuji Station in 1996. The Antarctic micrometeorite

working group collected MMs from the deposits and has been studying them by various methods such as synchrotron radiation induced XRF, XRD, EPMA, SEM, TEM, noble gas analysis, INAA, and ion microprobes (Noguchi *et al.*, 2000). In this study, six unmelted MMs which were thought to be weakly to moderately heated were investigated by transmission electron microscopy (TEM). Among the six MMs there is one phyllosilicate-bearing MM, which was found by the X-ray diffraction analysis (Nakamura *et al.*, in preparation). Its mineralogy is compared with that of a phyllosilicate-bearing MM which was investigated by a TEM in the study of Klöck and Stadermann (1994). Variation of mineralogy among dehydrated MMs was investigated in detail. It was found that two MMs contained terrestrial weathering products. It is thought that phyllosilicates in MMs were decomposed to aggregates of anhydrous minerals (olivine, magnetite, and low-Ca pyroxene) about 700°C (Greshake *et al.*, 1996, 1998). In this study, an assemblage of low-Ca pyroxene and (Mg, Fe)O was found in two MMs which had experienced weak heating. We will briefly discuss dehydration processes by heating during atmospheric entry.

2. Samples and methods

MMs investigated in this study were selected both on the basis of qualitative analysis and observation of their surfaces by low-vacuum scanning electron microscopes (LV-SEMs) with EDS and on the basis of textural observation and quantitative analysis of their sections by a SEM and an electron microprobe analyzer (EPMA). Selected unmelted MMs were investigated by a Gandolfi camera in order to study bulk mineralogy of each MM (Nakamura *et al.*, in preparation). After investigation by Gandolfi X-ray camera, each MM was embedded in epoxy resin and microtomed by Leitz-Reihert Super Nova ultramicrotome for transmission electron microscope (TEM) observation. Microstructure and mineralogy of each MMs were obtained by JEOL JEM-2000FX II with Philips DX-4 EDS. For quantitative analysis, the Cliff-Lorimer thin film approximation was used for data reduction. Experimental k factors were determined from many mineral standards. Effects of sample thickness on k factors were considered by regarding k factors as functions of peak intensities. Remainders of embedded MM were observed by LV-SEMs, JEOL JSM-5300LV with Oxford ISIS 300 EDS and JEOL JSM-5900LV with Oxford ISIS 310 EDS for textural observation and qualitative analysis. The reason why LV-SEMs were used is that observation and analysis of each MM can be performed without carbon coating, which may affect the quality of ultrathin sections if the remainders of the MM samples are ultramicrotomed again based on the SEM data. After TEM and SEM investigation, the MMs were coated by carbon, and their chemical compositions were obtained by JEOL JXA-733 EPMA operated at 15 kV accelerating voltage and 9 nA beam current. Detection limits of EPMA analysis based on the Bence and Albee correction for minor elements (wt%) were reported in Noguchi (1995).

3. Results

In the consortium study of AMMs collected at the Dome Fuji Station, more than 230 MMs were recovered and investigated. Among them, 83 MMs were investigated by Gandolfi X-ray camera and/or SEM and EPMA in order to select MMs for TEM study. The authors selected six MMs for this study. Among them, five MMs which were thought to have experienced weak to relatively weak heating during atmospheric entry were selected based on their morphology and qualitative analyses of their surfaces. However, their bulk mineralogy and textures and chemical compositions of their cross sections revealed that the extent of heating during atmospheric entry varies; weakly to moderately heated. Also the authors searched weakly heated MMs among those investigated by a SEM and an EPMA. Among them, one MM which was thought to have experienced relatively weak heating was selected for this study.

3.1. Texture, bulk mineralogy, and chemical compositions of the MMs

A backscattered electron image (BEI) of F96CI024 shows that this MM has a compact matrix. The matrix is composed of very fine-grained (sub-μm sized) minerals and some coarse-grained (5 to 20 μm across) Fe oxide and sulfides (Fig. 1a). This MM contains a plaquette magnetite aggregate, but does not contain framboidal magnetite. One euhedral pentlandite grain was found as well as pyrrhotite. Anhydrous silicates were not observed in this MM. Based on the X-ray diffraction data, F96CI024 is composed mainly of saponite, pyrrhotite, and magnetite and that olivine and low-Ca pyroxene are very minor components in this MM (Nakamura *et al.*, in preparation). It has a strong diffraction peak at about 0.97 nm that is attributed to (001) reflection of saponite. A diffraction peak at 0.45 nm is attributed to (02 *l*) prism reflection due to stacking disorder of saponite (Nakamura *et al.*, in preparation). The Si-Mg-Fe diagram suggests that the MM is a mixture of saponite with the Mg/(Mg + Fe) ratio around 0.7 and the average Al_2O_3 content of 2.8 wt%, and Fe-rich phases (Fig. 2a).

The other five MMs have various textures although they are similar in mineralogy to each other except their crystallinity and relative abundances. X-ray diffraction data of F96CI020 and F96DI021 suggest that anhydrous minerals in the two samples are very fine and contain a mineral in common which have a diffraction peak at 0.628 nm (Nakamura *et al.*, in preparation). However, their textures and chemical compositions are different from each other. A BEI of F96CI025 shows that the matrix of the MM is porous and composed of fine-grained (sub-μm sized) minerals with large (10 to 15 μm across) relict olivine (Fo96 to 98) and kamacite (Fig. 1b). X-ray diffraction data suggest that F96CI025 is composed mainly of pyrrhotite and very fine-grained olivine and low-Ca pyroxene and that does not contain phyllosilicates (Nakamura *et al.*, in preparation). Chemical composition of the MM suggests that it is composed mainly of olivine and magnetite although only a few analyses could be done due to its high porosity. On the other hand, a BEI of

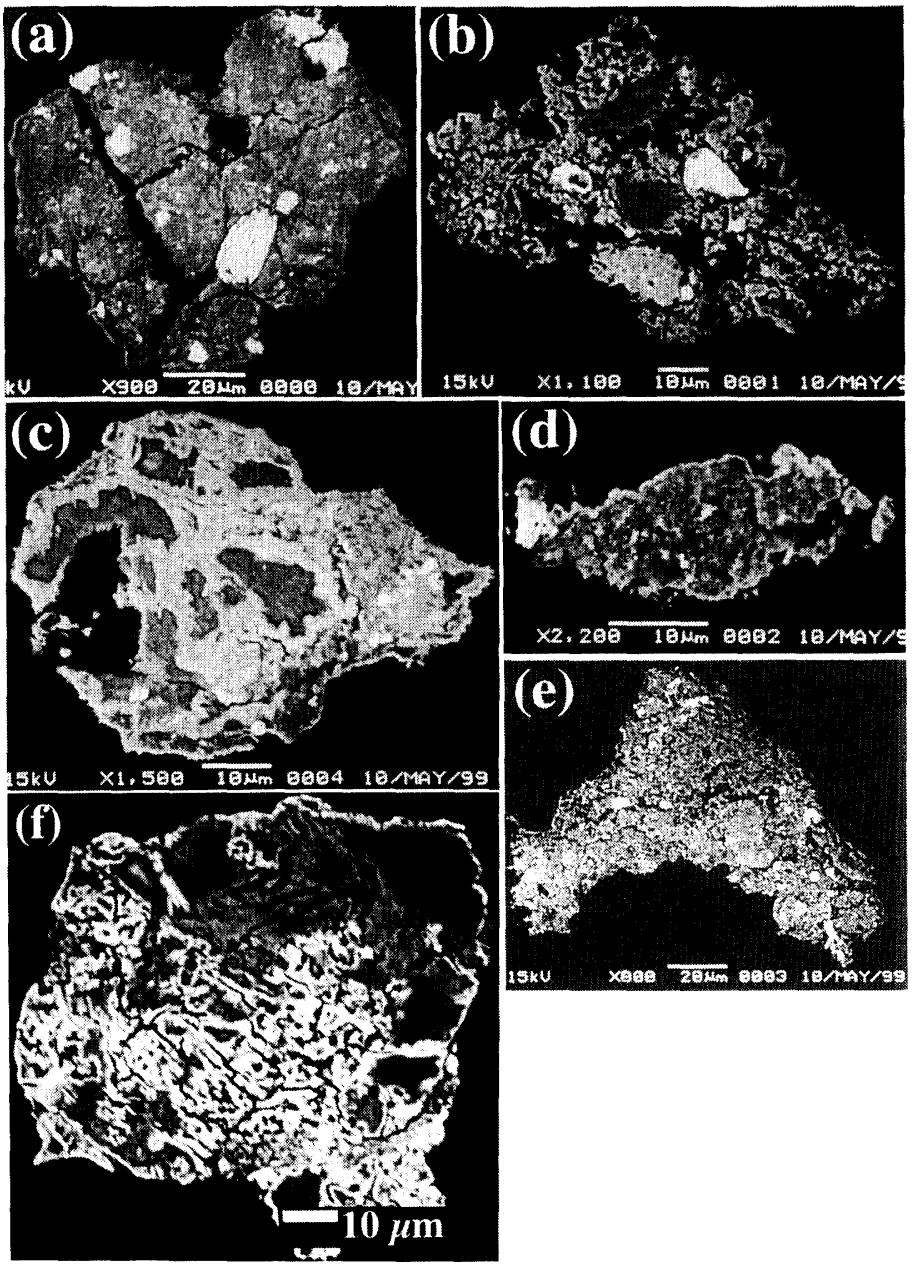

Fig. 1. Backscattered electron images (BEIs) of cross sections of micrometeorites (MMs) investigated by X-ray and TEM. These samples are the remainders after ultrathin sections were cut by an ultramicrotome. After ultramicrotomy by a diamond knife, the surfaces of MMs are very flat as if polished by diamond paste. (a) F96CI024: a phyllosilicate-bearing MM. A plaquette magnetite (bright large grain) is found in the middle of the photograph. The other coarse bright grains are magnetite, pyrrhotite, and pentlandite. (b) F96CI025: a porous dehydrated MM. Relict olivine (two dark grains) and kamacite (one bright grain) are observed. (c) F96CI020: a dehydrated MM with compact matrix, showing dark cores and bright rims. (d) F96DI021: a dehydrated MM (scoriaceous). Bright rim is observed on the periphery of the MM. (e) F96DI045 a dehydrated MM (scoriaceous). (f) F96DK056, a dehydrated MM, showing dark cores and bright rims.

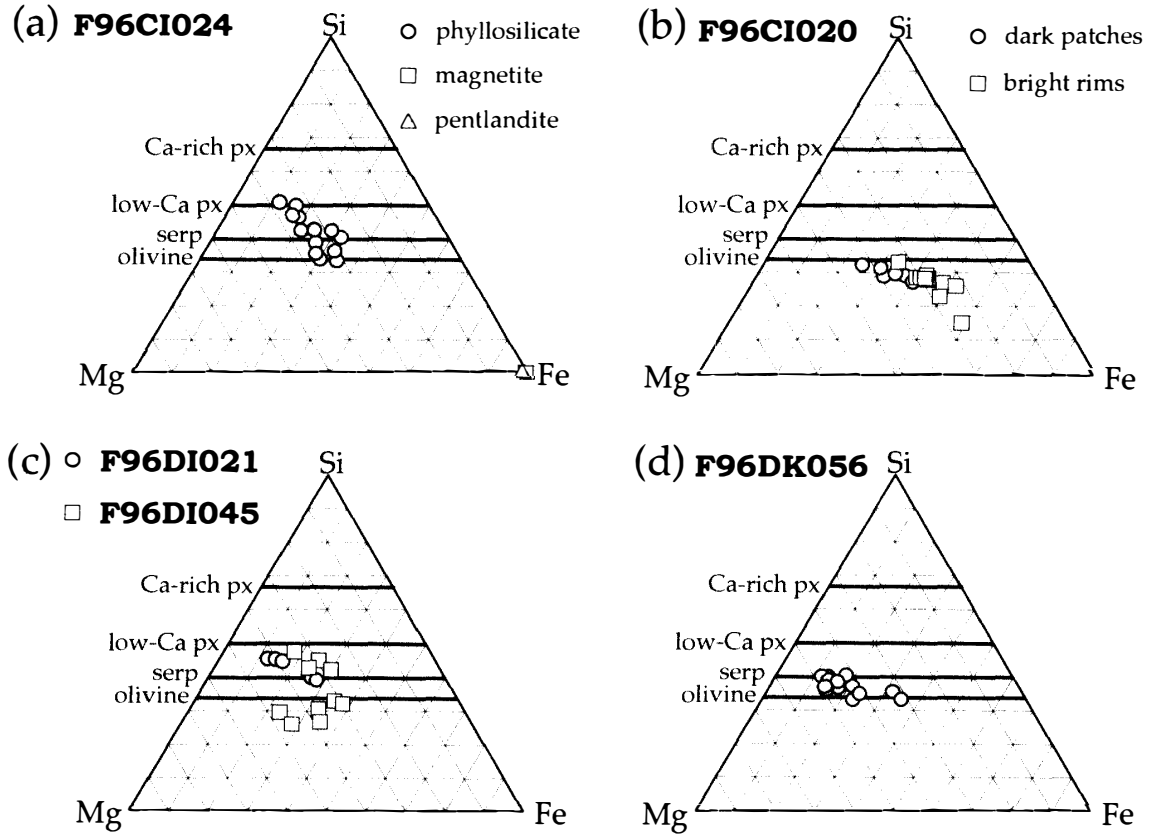

Fig. 2. Si-Mg-Fe diagrams of matrices and some coarse relict minerals in five MMs. These data were obtained by focused beam. (a) F96CI024, (b) F96CI020, (c) F96DI021 and F96DI 045, and (d) F96DK056. Abbreviations. low-Ca px: low-Ca pyroxene; Ca-rich px: Ca-rich pyroxene; serp: serpentine.

F96CI020 displays that the MM has a fine-grained (sub-μm sized) compact matrix (Fig. 1c). The MM has dark patches and bright rims in the BEI. X-ray diffraction analysis indicates that F96CI020 is composed of very fine-grained olivine and magnetite, and amorphous material (Nakamura *et al.*, in preparation). The Si-Mg-Fe diagram suggests that the MM is composed mainly of olivine whose Mg/(Mg+Fe) ratio is around 0.6 and Fe-rich phases and that the difference between dark patches and bright rims results from the different ratios of olivine and Fe-rich phases between them (Fig. 2b).

BEIs of F96DI021 and F96DI045 show that they have similar textures to that of F96CI025. They are composed of porous aggregates of very-fine grained (sub-μm sized) minerals although they do not have relict minerals (Figs. 1d and 1e). X-ray diffraction of F96DI021 and F96DI045 revealed that they are composed mainly of fine-grained olivine, low-Ca pyroxene, and magnetite (Nakamura *et al.*, in preparation). If major element contents of these MMs were not changed greatly by heating during atmospheric entry, the Si-Mg-Fe diagram suggests that the matrices of the MMs were originally composed mainly of phyllosilicate and Fe-rich phases (Fig. 2c). Figure 2c also suggests that secondary olivine which was formed by dehydration of phyllosilicate are more abundant in F96DI045 than in F96DI021. In

the case of F96DI045, there are some analyses which are plotted below the solid solution line of olivine. Their compositions suggest that the MM contains minerals having higher Mg and Fe contents than those of olivine. This will be discussed later.

BEI of F96DK056 shows that the MM has a fine-grained (sub-μm sized) compact matrix (Fig. 1f). As is the case of F96CI020, the MM has dark patches and bright rims in the BEI. (Fig. 1f). There are no large grains of relict anhydrous minerals in the MM. X-ray diffraction of F96DK056 indicates that the MM is composed mainly of very fine-grained olivine, magnetite, and a small amount of Fe-sulfide. Weak intensity of diffraction peaks of minerals is probably attributed to abundant amorphous materials in the MM (Nakamura *et al.*, in preparation). Chemical composition of the matrix of this MM suggests that serpentine is preserved in this MM. The Si-Mg-Fe diagram also shows that the matrix of the MM has serpentine-like elemental ratios (Fig. 2d). However, X-ray diffraction data indicate that the MM is now dehydrated.

3.2. TEM observation of the MMs

TEM observation revealed that only one MM contains phyllosilicate. Population of MMs preserving phyllosilicate was 1/83 (1.2%) in this study. The others contain only anhydrous minerals except for minerals formed due to terrestrial weathering. They were thought to have contained phyllosilicates before entering the earth's atmosphere, based on their mineralogy and electron petrography. Anhydrous MMs which had phyllosilicates before atmospheric entry have textures characteristic of the dehydration of phyllosilicates (Klöck and Stadermann, 1994; Greshake *et al.*, 1996, 1998). Based on the previous studies of MMs, the other five MMs in this study were originally phyllosilicate-bearing before atmospheric entry. Major minerals which compose dehydrated MMs were olivine, magnetite, low-Ca pyroxene, Fe sulfides, magnesium- and iron-bearing oxide, and glassy material which fills the interstices of these anhydrous minerals. Their grain sizes and relative abundances change according to the extent of heating during atmospheric entry, as well as their positions within each MM.

(a) F96CI024

Figure 3a shows a low-magnification bright-field (BF) image of F96CI024. This photomicrograph displays that the matrix of this MM is not porous and composed of sub-μm sized phyllosilicate with finely dispersed sub-μm sized magnetite, pyrrhotite, and a Mg- and Fe-bearing mineral. Subhedral magnetite and pentlandite grains more than 2 μm across are shown in Fig. 3a. Phyllosilicate grains in this MM are curved and have a thickness of >20 nm (Fig. 3b). The lattice fringes contain many stacking disorders. High-resolution images of the phyllosilicate reveal that it has 0.97 to 0.98 nm lattice fringes (Fig. 3b), and the spacing of the fringes indicates that the phyllosilicate is saponite. The fringes are often dim even in high-resolution images. Figure 3d is a selected area electron diffraction (SAED) photograph, where the contrast of the photograph is enhanced by an image processing software. Diffraction spots shown in this figure correspond to diffraction from the basal plane of saponite. The diffraction spots indicate that the spacing of

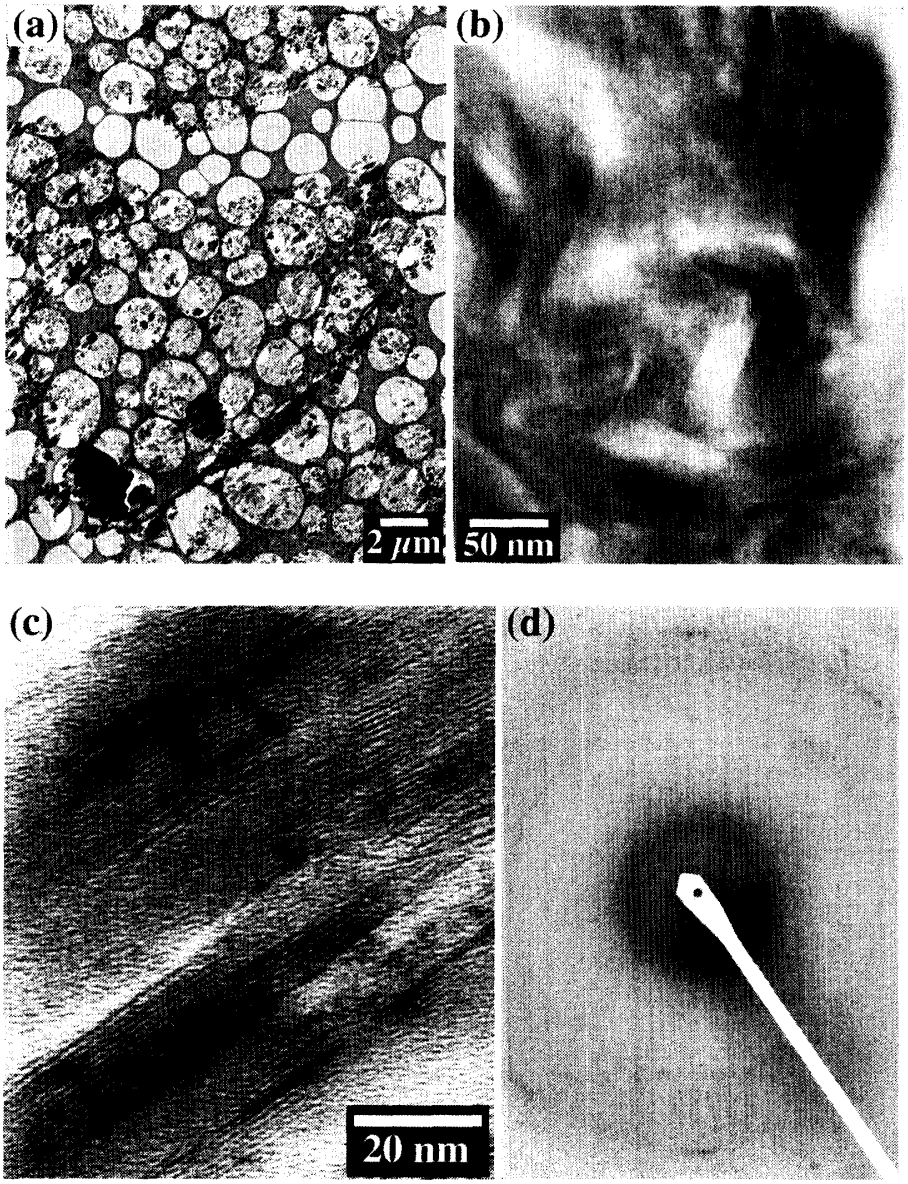

Fig. 3. TEM photomicrographs of F96CI024. (a) A low-magnification bright-field (BF) image. The matrix of this MM is composed of abundant phyllosilicate and embedded fine-grained magnetite and Fe-sulfides. Two large mineral grains (lower left) are magnetite and pentlandite. Honeycomb-like networks in Figs. 3 to 7 are thin plastic films which support ultrathin sections of MMs. (b) Phyllosilicate in the MM. Phyllosilicate crystals are relatively coarse. Their thickness perpendicular to the fringes is >20 nm. (c) High-resolution image of the phyllosilicate. It shows 0.97 to 0.98 nm lattice fringes. The phyllosilicate is saponite. (d) Selected area electron diffraction (SAED) image of the phyllosilicate. Diffraction spots from the phyllosilicate are weak in most cases. Diffraction spots in this photographs are enhanced by an image processing software. These diffraction spots correspond to those from the basal planes of saponite.

basal planes of saponite is 0.98 nm. Diffraction spots of the phyllosilicate are rarely sharp in most of the SAED photographs. Serpentine, which has 0.7 nm lattice fringes, were not observed in the MM.

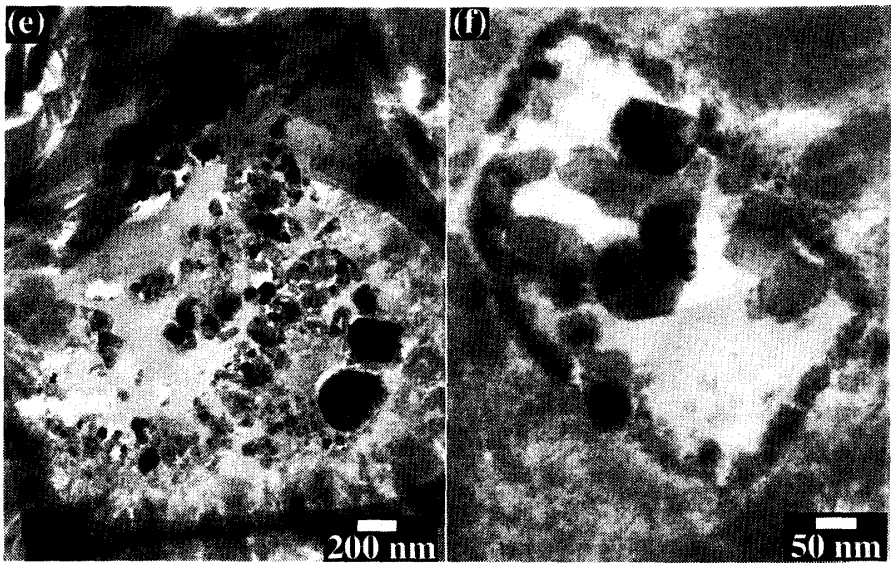

Fig. 3 (continued). (e) and (f) Aggregates of magnetite, Fe-sulfides, and a Mg- and Fe-bearing mineral. These minerals occur as aggregates in this MM. These aggregates are surrounded by coarse phyllosilicate grains. Some aggregates have fine-grained rims, as shown in (f).

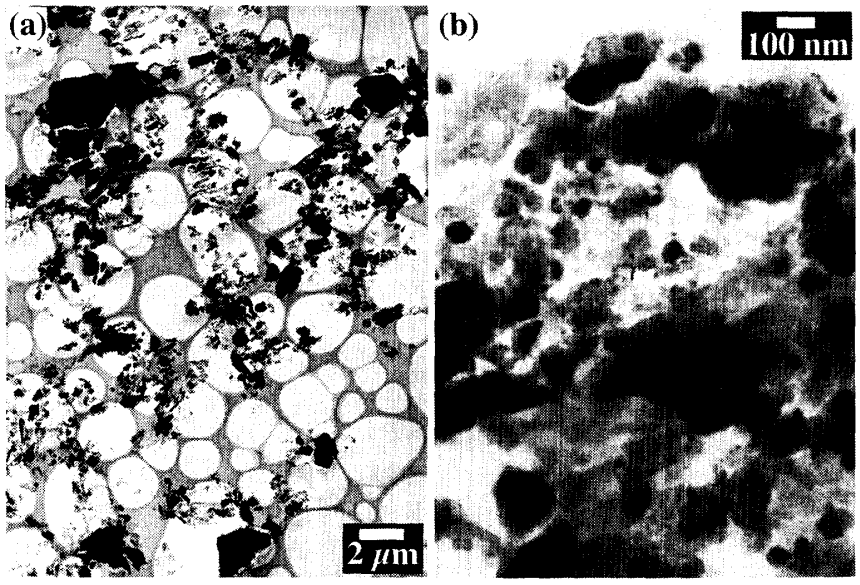

Fig. 4. TEM photomicrographs of F96CI025. (a) A low-magnification BF image. This photograph shows that the matrix is very porous. (b) The matrix of this MM is composed of coarse- and fine-grained anhydrous minerals such as olivine, pyrrhotite, magnetite, and low-Ca pyroxene.

As shown in Fig. 3a, sub-μm sized magnetite, pyrrhotite, and pentlandite were embedded in the matrix of the MM. These Fe oxide and sulfides occur as aggregates (Figs. 3e and 3f). These aggregates are 0.5 to 2 μm across and surrounded by bundles of phyllosilicates. Some aggregates have definite rims (Fig. 3f).

(b) F96CI025

As displayed by Fig. 1b, a low-magnification BF image of F96CI025 shows that

the MM has a very porous matrix (Fig. 4a). This photomicrograph shows that the matrix contains abundant minerals of 0.5 to 2 μm in diameter. These coarse-grained minerals are embedded in fine-grained ($<$200 nm across) minerals (Fig. 4b). Average grain size of these anhydrous grains is about 60 nm. Coarse-grained minerals are olivine, pyrrhotite, and magnetite. Fine-grained minerals include low-Ca pyroxene in addition to minerals found in coarse-grained minerals. Most of the fine-grained olivine has Fo50 to 60. On the other hand, coarse-grained olivine has Fo93 to 99. A small amount of Ca-rich pyroxene and glassy (or amorphous) material were observed in the fine-grained areas.

(c) F96CI020

A low-magnification BF image of F96CI020 shows that the matrix of the MM is very fine-grained and not porous (Fig. 5a). Very fine-grained areas in this figure correspond to dark cores in the BEI of the MM (Fig. 1b). As shown in Fig. 5b, the dark cores are composed of minerals $<$100 nm in diameter, and do not contain coarse ($>$0.5 μm across) minerals observed in the matrix of F96CI025. Average grain size of these minerals is about 30 nm. They are abundant olivine, magnetite, pyrrhotite, and amorphous material. Most of the olivine has Fo30 to 55. Bright rims in the BEI of the MM in Fig. 1b occur as black rims in Fig. 5a.

Figure 5c is a BF image of a rim of this MM, and Fig. 5d is a close-up of the rim. As shown in Fig. 5d, the rims contain abundant fibrous minerals with $<$10 nm wide. High-resolution image of such fibrous minerals reveal that the mineral has 0.63 to 0.65 nm lattice fringes. The major element of the mineral is iron. Glassy (or amorphous) material was observed among the fibrous mineral grains.

(d) F96DI021

F96DI021 is composed mainly of fine-grained olivine, pyrrhotite, magnetite, and low-Ca pyroxene. Figure 6a shows a low magnification BF image of F96DI021. This photomicrograph displays that the matrix of this MM is porous and composed of anhydrous minerals such as olivine, pyrrhotite, and magnetite. Average grain size of the anhydrous minerals is about 70 nm. Figure 6b shows that there are many mineral grains $>$100 nm across, and that glassy (or amorphous) material in the interstices of the mineral grains is more abundant than that in the others. In the figure, fibrous materials are observed in the glassy material.

These fibrous materials are observed in the interior and the rim of the MM (Figs. 6c and d). They are more abundant in the rim than in the interior. The fibrous materials have lattice fringes with intervals of 0.63 to 0.65 nm in both the interior and the rim. Thickness of the fibrous materials are 5 to 10 nm. The major element of the fibrous mineral is iron as well as a similar mineral in F96CI020.

(e) F96DI045

The matrix of F96DI045 is also porous (Fig. 7a). The peripheries of the MM are composed mainly of fine-grained olivine, pyrrhotite, and magnetite. However, the interior of the MM is composed mainly of low-Ca pyroxene and magnesium- and an iron-bearing mineral. The Mg/(Mg + Fe) ratios of low-Ca pyroxene are 0.6 to 0.8. Selected area electron diffraction patterns of the magnesium- and iron-bearing mineral suggest that it is (Mg, Fe)O. Their Mg/(Mg + Fe) ratios are 0.5 to 0.6. In

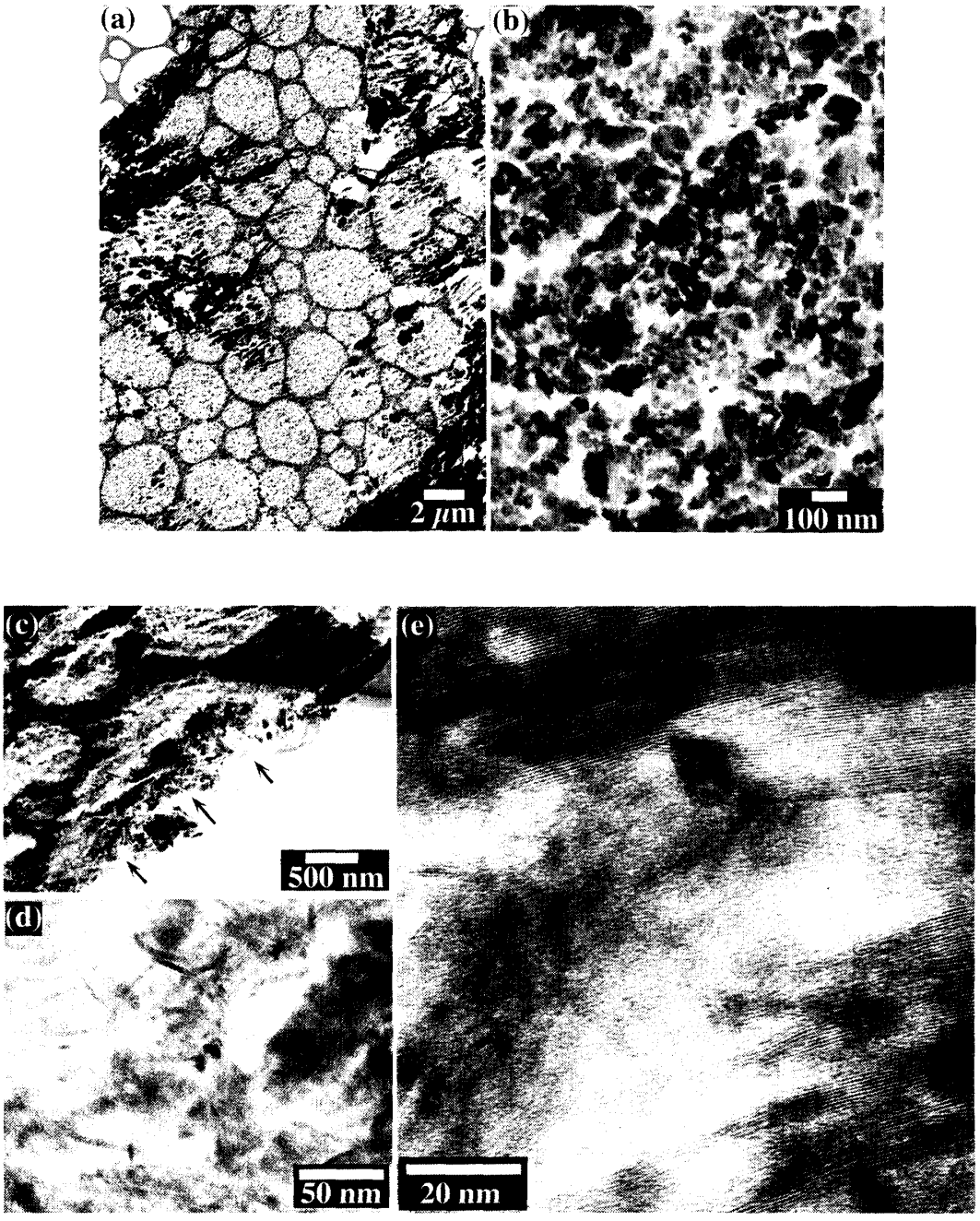

Fig. 5. TEM photomicrographs of F96CI020. (a) A low-magnification BF image. This photograph shows that the matrix is compact and composed of fine-grained anhydrous minerals. Darker areas (middle left and right edge of the photograph) correspond to the bright rims in BEI photographs in Fig. 1 (c). The other dark areas (upper left and lower right) are artifacts due to folding of an ultrathin section. (b) The matrix of this MM is composed of fine-grained anhydrous minerals such as olivine, magnetite, and pyrrhotite. Low-Ca pyroxene is rare. (c) The rim of F96CI020 is indicated by arrows. (d) An enlarged view of the rim in (c). fibrous minerals are observed. (e) High-resolution image of the fibrous and tabular minerals. They have 0.63 to 0.65 nm lattice fringes.

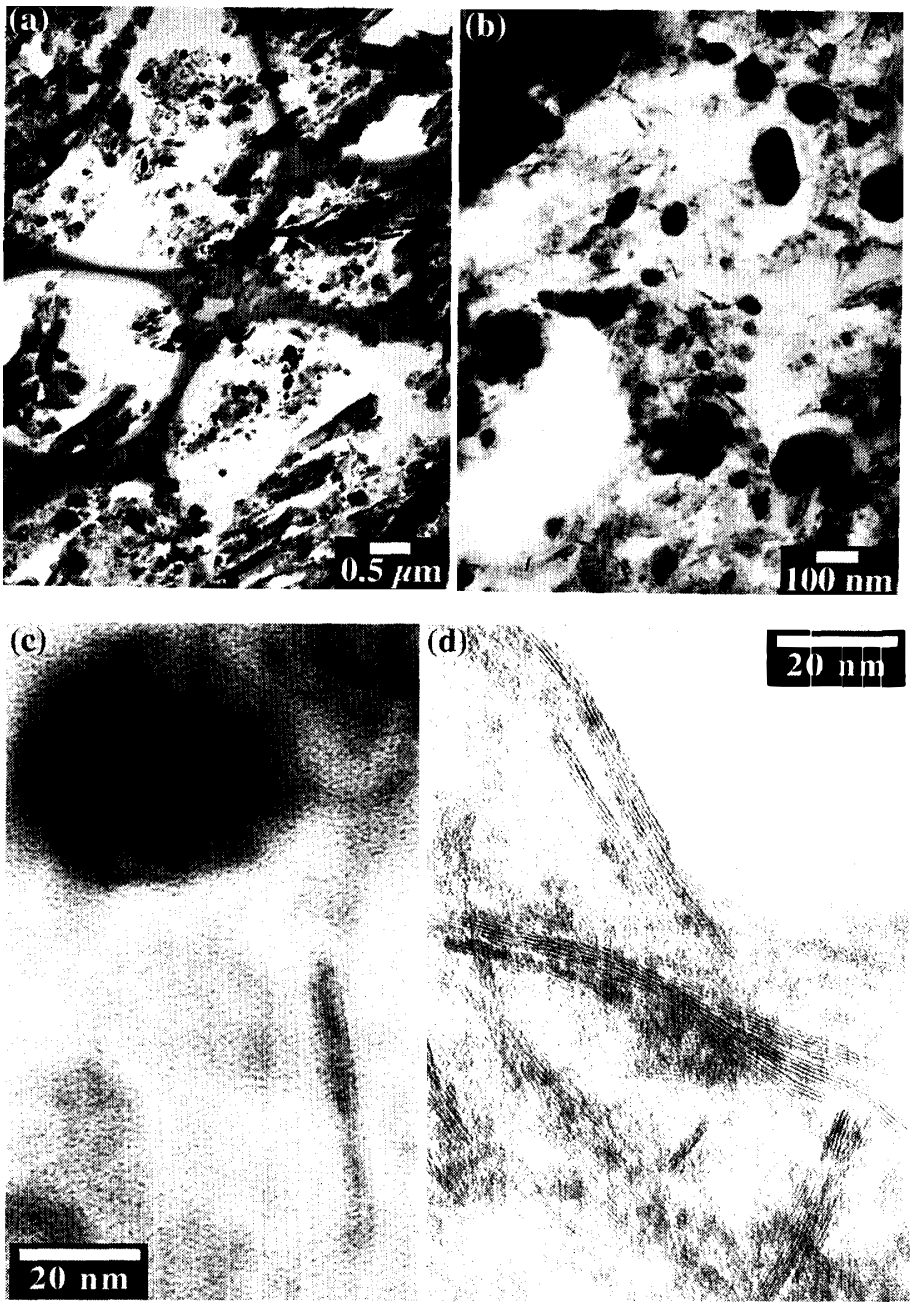

Fig. 6. TEM photomicrographs of F96DI021. (a) A low-magnification BF image. This photograph shows that the matrix is porous and composed of relatively coarse-grained anhydrous minerals. (b) The matrix of this MM is composed of relatively coarse-grained anhydrous minerals such as olivine, pyrrhotite, magnetite, and low-Ca pyroxene and interstitial glassy (or amorphous) material. Some fibrous grains are observed. (c) Fibrous minerals in the interior of the MM. (d) Fibrous minerals in the rim. It is more abundant in the rim than in the interior. Fibrous minerals in both (c) and (d) have 0.63 to 0.65 nm lattice fringes.

Fig. 2c, there are analyses plotted below the solid solution line of olivine. The analyses probably resulted from abundant (Mg, Fe)O in the analyzed areas. Average grain size of the fine-grained minerals is about 50 nm. There is a small

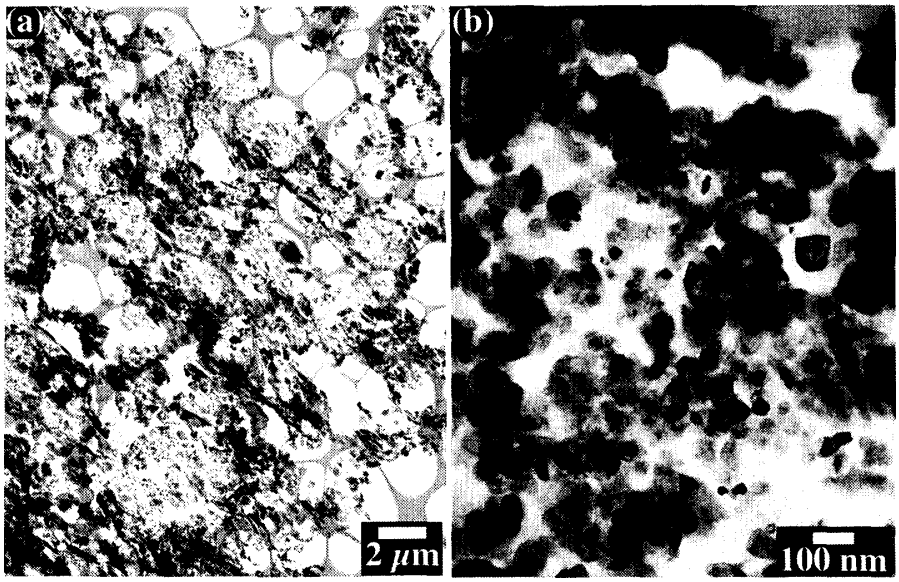

Fig. 7. TEM photomicrographs of F96DI045. (a) A low-magnification BF image. This photograph shows that the matrix is porous and composed of anhydrous minerals. (b) The matrix of the interior of this MM is composed mainly of fine-grained (Mg, Fe)O (high contrast grains in this figure) and low-Ca pyroxene.

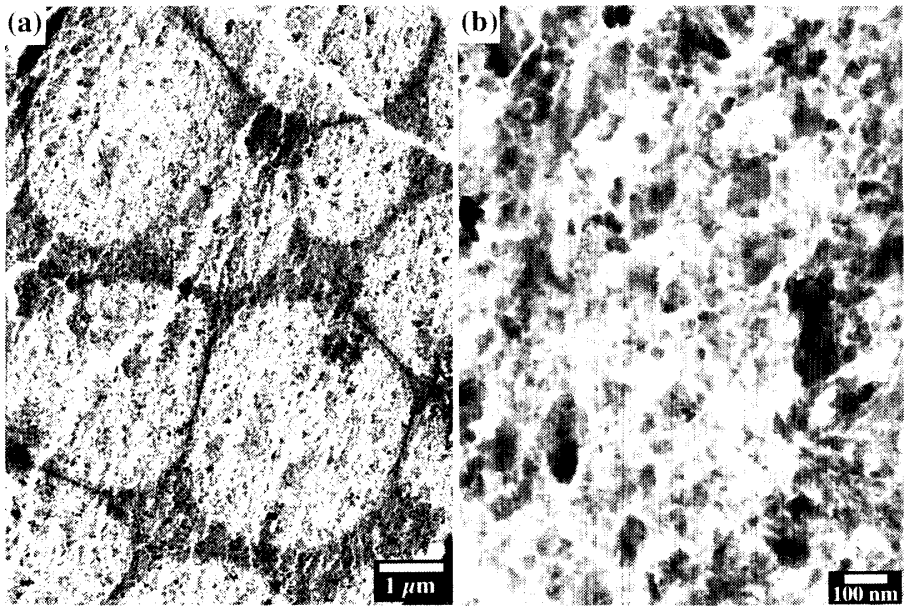

Fig. 8. TEM photomicrographs of F96DK056. (a) A low-magnification BF image. This photograph shows that the matrix is compact and composed of fine-grained anhydrous minerals. (b) The matrix of this MM is composed of fine-grained olivine, magnetite, and pyrrhotite.

amount of Ca-rich pyroxene and glassy material among the anhydrous minerals. It is interesting to note that a Ca-rich pyroxene crystal containing about 12 wt% Al_2O_3 and 6.5 wt% TiO_2 was found. As it is almost Fe-free, it may be a relict crystal.

(f) F96DK056

A low-magnification BF image of F96DK056 shows that the matrix of the MM is very fine-grained and not porous (Fig. 8). The area displayed in this figure corresponds to dark areas in the BEI of the MM (Fig. 1f). The matrix is composed of anhydrous minerals such as olivine, magnetite, and pyrrhotite, and amorphous material. Average grain size of these minerals is about 40 nm. Low-Ca pyroxene is rare but concentrated in places. A small amount of (Mg, Fe)O coexists with low-Ca pyroxene.

4. Discussion

4.1. Mineralogy and petrology of F96CI024

F96CI024 is the only MM which has a completely hydrated mineral assemblage in the consortium study. Saponite was observed but serpentine was not in F96CI 024. Relict anhydrous minerals are virtually absent except for Fe oxide and sulfides. Texture and mineralogy of this MM are similar to those of a phyllosilicate-rich AMM, BI91/3-108 (Kurat *et al.*, 1992; Klöck and Stadermann, 1994). Aggregates of magnetite, Fe-sulfides, and (Mg, Fe)O (each grain is <100 nm across, most of them are <50 nm) were found during TEM observation (Figs. 3e and 3f). However, such aggregates were not reported on BI91/3-108. In the matrix of BI91/3-108, rounded Fe-sulfide grains were embedded in saponite grains (Klöck and Stadermann, 1994). On the other hand, framboidal magnetite which was found in BI91/3-108 was not found in F96CI024. As shown above, both MMs are composed of abundant saponite, magnetite, and Fe-sulfides, although there is textural difference between them. Chemical compositions of saponite in these two MMs are very similar to each other. Their Mg/(Mg+Fe) ratios are around 0.7. Phyllosilicate mineralogy and their chemical compositions are different from those of CI, CM, and CR chondrites. In these chondrites, matrices are composed of saponite and serpentine, only serpentine, and serpentine and chlorite (*e.g.* Tomeoka *et al.*, 1989; Buseck and Hua, 1993; Weisberg *et al.*, 1993). Matrices of two hydrated CV chondrites, Kaba and Mokoia contain saponite without serpentine. However, the saponite in them is more magnesian than that in the two MMs (Keller and Buseck, 1990; Tomeoka and Buseck, 1990; Klöck and Stadermann, 1994). Klöck and Stadermann (1994) reported that mineralogy and texture of the matrix of BI91/3-108 are similar to those of Semarkona LL3.0 chondrite. Mineralogy and texture of the matrix of F96CI024 are also similar to those of Semarkona, although magnetite, Fe-sulfide, and (Mg, Fe)O aggregates were also not reported in Semarkona (Alexander *et al.*, 1989; Klöck and Stadermann, 1994). From the standpoint of mineralogy, it is suggested that parent bodies of these MMs are different from parent bodies of CI, CM, CR, and hydrated CV chondrites, but that conditions for aqueous alteration in these MMs (and perhaps Semarkona) are similar to each other.

4.2. *Effect of heat during atmospheric entry of F96CI024 and the other MMs investigated*

Irrespective of the measuring methods used (X-ray or TEM), measured spacing of (001) of saponite in F96CI024 is almost identical: 0.97 nm by Gandolfi X-ray camera (Nakamura *et al.*, in preparation) and 0.97–0.98 nm by SAED photographs. X-ray measurement was performed under the atmospheric condition (Nakamura *et al.*, in preparation). On the other hand, SAED photographs were taken under vacuum condition. These data mean that saponite in this MM was dehydrated before investigation. Broad peaks of saponite in X-ray diffraction (Nakamura *et al.*, in preparation), scarcity of saponite crystals with sharp lattice fringes in high-resolution electron photomicrographs and with sharp diffraction spots in SAED photographs indicate that saponite in the MM still retains their crystal structure but that their structure has been disturbed by dehydration of interlayer H_2O.

In heating experiments, when phyllosilicates in CI chondrites Orgueil and Alais were heated for 20 sec to 700°C, crystal structures of the phyllosilicates were lost but their fibrous appearance were kept (Greshake *et al.*, 1998, 1996). Because saponite in the MM keeps their sheet structure, it was not heated to 700°C during atmospheric heating. Dehydration of interlayer H_2O in saponite is lost when heated to 200 to 300°C. In this case, sheet structure of saponite is kept although disturbed. Characteristics of phyllosilicate in the MM coincide with this case. It is suggested that the MMs were heated to relatively low temperatures (probably 200 to 300°C) during atmospheric heating.

TEM study of the MMs except for F96CI024 shows that they do not contain phyllosilicates even in a trace amount. In heating experiments, when phyllosilicates in CI chondrites Orgueil and Alais were heated for 20 sec to 800°C, texture of the phyllosilicates was lost and recrystallized to anhydrous minerals (Greshake *et al.*, 1998, 1996). Grain sizes of newly formed minerals in the experiment are 100 to 150 nm (Greshake *et al.*, 1998), which is larger than those observed in the dehydrated MMs. Therefore, duration of heating and maximum temperature during atmospheric entry of these dehydrated MMs were probably lower and/or shorter than the case of the experiment described above (heated for 20 sec to 800°C). In this study, it was found that (Mg, Fe)O coexists with low-Ca pyroxene in low-Ca pyroxene-rich areas in F96DI045 and F96DK056. The mineral assemblage has not been reported in previous studies (Klöck and Stadermann, 1994; Greshake *et al.*, 1998, 1996). In these two MMs, previously reported mineral assemblage (olivine, magnetite, and low-Ca pyroxene) was observed in the rims which suffered more heating during atmospheric entry. Although the observed mineral assemblage and its texture suggest that these minerals were formed during dehydration of phyllosilicates during atmospheric entry, further study is needed to clarify the origin of these minerals.

4.3. *Terrestrial weathering of AMMs on the earth (in polar ice)*

In F96CI020, fibrous and tabular minerals were observed in the rim of the MM.

Despite their morphological difference, their spacing of lattice fringes are the same: 0.63 to 0.65 nm. In F96DI021, fibrous minerals with lattice fringes of 0.63 to 0.65 nm were also observed both in the rim and in the interior. They are more abundant in the rim than in the interior. Unidentified diffraction peak at 0.628 nm in Gandolfi analysis probably resulted from the diffraction from these fibrous and tabular minerals. Their occurrences suggest that the minerals were formed during terrestrial weathering of the glassy material of the MMs. EDS spectra of these minerals indicate a high Fe content. Their chemical compositions and lattice fringes suggest that the minerals are lepidocrocite: γ-FeOOH. (020) of γ-FeOOH has the spacing of 0.63 nm. It coincides with the spacing of the lattice fringes. Lepidocrocite displaying (020) lattice fringes is typical for the smallest lepidocrocite crystals (Cornell and Schwertmann, 1996).

The existence of lepidocrocite in these MMs indicates that some MMs are very susceptible to suffer terrestrial weathering even kept in ice (or snow). The snow in which MMs were embedded fell during 1950s to 1970s (Nakamura *et al.*, 1999). It is suggested that the two MMs were aqueously altered in the snow during 30 to 50 years. In AMMs collected in 1991 by Maurette and his colleagues, olivine crystals with planar defects subparallel to (001) were observed (Yano and Noguchi, 1998). The microstructure shown in olivine is typical for the initial stage for iddingsitization of olivine (Smith *et al.*, 1987). The microstructure indicating iddingsitization was not observed in olivine in the MMs investigated in this study. The MMs displaying iddingsitization were recovered from blue ice. The duration preserved in ice (or snow) is probably much longer in the case of the 1991 Maurette's sample than in the case of the Dome Fuji sample. The above data suggest that the rims of MMs were weathered in snow (or ice) in relatively short duration. The occurrence of olivine with planar defects suggests that olivine formed by dehydration of phyllosilicates was also weathered in ice when MMs were kept in ice (or snow) for a long time. However, because not all the MMs collected at the same sampling site show the same extent of terrestrial weathering, other parameters such as temperature of MMs when they were warmed up by sunlight at or near the surface of snow may also have been affected the extent of weathering.

4.4. Population of phyllosilicate-bearing MMs in this study

In previous studies, 6 to 16% of MMs contain phyllosilicate (Kurat *et al.*, 1992; Genge *et al.*, 1997). On the contrary, only one MM contains phyllosilicate among 83 MMs investigated by X-ray diffraction, TEM, SEM, and EPMA in this consortium study. Because these MMs were collected at several laboratories (Noguchi *et al.*, 2000), it is difficult to understand this inconsistency as a sampling bias. There are two possible explanations for this discrepancy. The first explanation is that the discrepancy is apparent. In this study, all the MMs which were regarded as phyllosilicate-bearing based on SEM and EPMA data were investigated by TEM. During "cross-check" of candidates of phyllosilicate-bearing MMs, some MMs such as F96DK056 were revealed to be anhydrous. Therefore, there may be a possibility that the population of phyllosilicate-bearing MMs was overestimated in previous

studies. The second explanation is that population of phyllosilicate-bearing MMs change with time. MMs which enter the atmosphere with relatively low velocity to the earth experience relatively low maximum temperature during atmospheric entry. If such MMs contain phyllosilicate, it will survive after atmospheric entry. However, we cannot check the idea because of the lack of data for flux change of MMs.

5. Conclusions

We investigated AMMs that experienced weak heating during atmospheric entry by TEM. Major mineral phases estimated by using the Gandolfi camera (Nakamura *et al.*, in preparation) correspond well to mineralogical data obtained by TEM.

We found a phyllosilicate-rich MM, F96CI024, which has similar texture and mineralogy of a saponite-bearing MM BI91/3-108 reported by Kurat *et al.* (1992) and Klöck and Stadermann (1994). Phyllosilicate in the MM F96CI024 is 1 nm-phyllosilicate (saponite), and serpentine was not observed as well as the case of BI 91/3-108. Their mineralogy suggests that they are different from CM, CI, CR, and hydrated CV chondrites.

Saponite in F96CI024 preserves their sheet-like structure, but the interlayer H_2O is dehydrated. The MM was probably experienced several hundreds $^\circ$C during atmospheric entry.

The other MMs does not contain phyllosilicates even in a trace amount. During the AMM consortium study, only one phyllosilicate-bearing MM was found among 83 MM investigated by X-ray, TEM, SEM, and EPMA.

F96DI045 and F96DK056 show a mineral assemblage of low-Ca pyroxene and (Mg, Fe)O in the areas abundant in low-Ca pyroxene.

F96DI021 and F96CI020 contain lepidocrocite. Lepidocrocite is observed within glassy material. Such material is susceptible to suffer terrestrial weathering even in snow (or ice).

Acknowledgments

The authors appreciate N. Imae for using the data of F96DK056. SEM observation of the MM samples was performed at Tokyo Institute of Technology and at National Institute of Polar Research. We thank H. Yurimoto at TITech and A. Yamaguchi and H. Kojima at NIPR for their permission to use LV-SEMs. The authors thank W. Klöck and M. Miyamoto for their constructing comments. The authors thank T. Hiroi and A. J. Martin for their cooperation to improve our text.

References

Alexander, C. M. O'D., Hutchison, R. and Barber, D. J. (1989): Origin of chondrule rims and interchondrule matrices in unequilibrated ordinary chondrites. Earth Planet. Sci. Lett., **95**, 187–207.

Buseck, P. R. and Hua, X. (1993): Matrices of carbonaceous chondrite meteorites. Ann. Rev. Earth

Planet. Sci., **21**, 255–305.

Cornell, R. M. and Schwertmann, U. (1996): The Iron Oxides. Weinheim, VCH, 573 p.

Genge, M. J., Grady, M. M. and Hutchison, R. (1997): The texture and compositions of fine-grained Antarctic micrometeorites: Implications for comparisons with meteorites. Geochim. Cosmochim. Acta, **61**, 5149–5162.

Greshake, A., Klöck, W., Arndt, P., Maetz, M. and Bischoff, A. (1996): Pulse-heating of fragments from Orgueil (CI): Simulation of atmospheric entry heating of micrometeorites. The Cosmic Dust Connection, ed. by J. M. Greenberg. Dordrecht, Kluwer Academic Publishers, 303–311.

Greshake, A., Klöck, W., Arndt, P., Maetz, M., Flynn, G. J., Bajt, S. and Bischoff, A. (1998): Heating experiments simulating atmospheric entry heating of micrometeorites: Clues to their parent body sources. Meteorit. Planet. Sci., **33**, 267–290.

Jessberger, E. K., Stephan, T., Rost, D., Arndt, P., Maetz, M., Stadermann, F. J., Brownlee, D. E., Bradley, J. P. and Krat, G. (1999): Properties of interplanetary dust: Information from collected samples. in press

Keller, L. P. and Buseck, P. R. (1990): Aqueous alteration in the Kaba CV3 carbonaceous chondrite. Geochim. Cosmochim. Acta, **54**, 2113–2120.

Klöck, W. and Stadermann, F. J. (1994): Mineralogical and chemical relationships of interplanetary dust particles, micrometeorites, and meteorites. Analysis of Interplanetary Dust, ed. by M. E. Zolensky *et al*. New York, Am. Inst. Phys., 51–87.

Kurat, G., Presper, T. and Brandstätter, F. (1992): CI-like micrometeorites from Cap Prudhomme, Antarctica. Lunar and Planetary Science XXIII. Houston, Lunar Planet. Inst., 747–748.

Kurat, G., Koeberl, C., Presper, T., Brandstätter, F. and Maurette, M. (1994): Petrology and geochemistry of Antarctic micrometeorites. Geochim. Cosmochim. Acta, **58**, 3879–3904.

Nakamura, T., Imae, N., Nakai, I., Noguchi, T., Yano, H., Terada, K., Murakami, T., Fukuoka, T., Nogami, K., Ohashi, H., Nozaki, W., Hashimoto, M., Kondo, N., Matsuzaki, H., Ichikawa, O. and Ohmori, R. (1999): Antarctic micrometeorites collected at the Dome Fuji Station. Antarct. Meteorite Res., **12**, 183–198.

Noguchi, T. (1995): Petrology and mineralogy of the PCA 91082 chondrite and its comparison with the Yamato-793495 (CR) chondrite. Proc. NIPR Symp. Antarct. Meteorites, **8**, 33–62.

Noguchi, T., Imae, N., Nakamura, T., Nozaki, W., Terada, K., Mori, T., Nakai, I., Kondo, N., Sasaki, M., Murakami, T., Fukuoka, T., Nogami, K., Ohmori, R. and Ohashi, H. (2000): A consortium study of Antarctic micrometeorites recovered from the Dome Fuji Station. Antarct. Meteorite Res., **13**, 270–284.

Smith, K. L., Milnes, A. R. and Eggleton, R. A. (1987): Weathering of basalt: Formation of iddingsite. Clays Clay Mineral., **35**, 418–428.

Tomeoka, K., McSween, H. Y., Jr. and Buseck, P. R. (1989): Mineralogical alteration of CM carbonaceous chondrites: A review. Proc. NIPR Symp. Antarct. Meteorites, **2**, 221–234.

Tomeoka, K. and Buseck, P. R. (1990) Phyllosilicates in the Mokoia CV carbonaceous chondrite: Evidence for aqueous alteration in an oxidizing environment. Geochim. Cosmochim. Acta, **54**, 1745–1754.

Yano, H. and Noguchi, T. (1998): Sample processing and initial analysis techniques for Antarctic micrometeorites. Antarct. Meteorite Res., **11**, 136–154.

Weisberg, M. K., Prinz, M., Clayton, R. N. and Mayeda, T. K. (1993): The CR2 (Renazzo-type) carbonaceous chondrite group and its implications. Geochim. Cosmochim. Acta, **57**, 1567–1586.

(Received October 6, 1999; Revised manuscript received January 28, 2000)